

ACTIVE CONTROL OF NEAR-WALL TURBULENCE WITH PERIODIC FORCING BY PLASMA ACTUATOR

S.Okochi, Y.Hasegawa, N.Kasagi and Y.Suzuki

Department of Mechanical Engineering, The University of Tokyo

7-3-1 Hongo, Bunkyo-ku, Tokyo, 113-8656, Japan

okouti@thtlab.t.u-tokyo.ac.jp

Abstract

An experimental study has been undertaken to reduce skin friction drag by applying spatially periodic forcing in the near wall region of a turbulent channel flow with micro plasma actuators. Measurements are made by a laser Doppler velocimeter (LDV) at $Re_\tau = 297$ and 602. We fabricate arrayed micro plasma actuators and reproduce spatially periodic control input assumed in the previous numerical simulation. However, the present plasma actuators induce a spanwise tangential velocity very close to the wall surface as we expect, but with considerable wall-normal velocities (blowing and suction). The latter effect cannot be neglected and should be taken into account for the turbulent drag reduction control in the future study.

1 Introduction

Predetermined control schemes for turbulent wall shear flows have been extensively investigated, because they have a possibility of achieving notable drag reduction despite their simple control algorithms. Various types of predetermined control schemes such as uniform (Quadrio et al., 2007) and sinusoidal (Yakeno et al., 2009) wall velocities have been proposed. Although intensive research efforts have been directed toward achieving turbulence drag reduction control over the decades, its real application still remains to be a difficult task because of lack of appropriate hardware components such as small enough actuators. Many actuators have been developed such as mechanical flaps and wall synthetic jets. These actuators have been successfully applied to mixing control in jet, separation control, and so forth. However, they cannot be readily applied to wall turbulence control because of their size, complex structure and energy consumption rate.

Roth et al. (1998) developed a plasma actuator by exploiting atmospheric pressure dielectric barrier discharge. Figure 1 shows the configuration of a typical plasma actuator. A plasma actuator consists of two metallic electrodes asymmetrically mounted on both sides of a dielectric plate and the lower electrode is covered with dielectric. A pulsed high

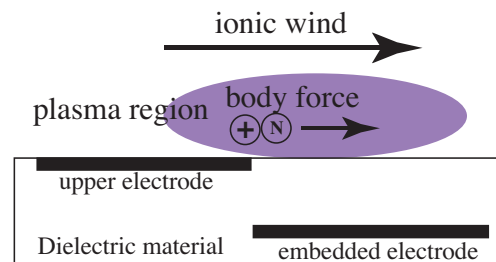


Figure 1: Structure of dielectric barrier discharge plasma actuator

voltage applied between the electrodes causes localized ionization of the air around the exposed electrode. In atmospheric pressure air, electric excitation at several kV and kHz is required to produce stable glow discharge plasma. Within the plasma region, localized forcing is produced due to the presence of charged particles within a highly non-uniform electric field. This force is transmitted to the ambient air through ion-neutral collisions, and results in a tangential flow induced a few millimetres away from the exposed electrode.

Okochi et al. (2009) fabricated micro plasma actuators for wall turbulence control through a MEMS process, and clarified the basic characteristics of the flow around the actuator. They showed that the maximum induced velocity, U_{max} , can be easily controlled by the applied voltage, driving frequency and electrode width. Achieving to fabricate micro plasma actuators by MEMS technique, it is possible to arrange them intricately, and to apply them to flexible flow control.

This study aims at experimentally achieving and validating the latest idea of turbulent drag reduction control, which has been proposed and assessed by numerical simulation. To do this, we fabricate and employ micro plasma actuators to mimic spatially periodic control input at the wall, and investigate the control effect by systematically changing the control parameters.

2 Experimental arrangement

2.1 Flow measurement

The experiment is carried out in a two dimensional turbulent channel, which is about 5 m

long with a cross section of $10 \times 50 \text{ cm}^2$. The Reynolds number based on the friction velocity, Re_τ , can be changed up to 750. In the present work, we consider two different Reynolds numbers, i.e., $\text{Re}_\tau = 297$ and 602. The streamwise and wall-normal velocity components, u and v , are measured by a laser Doppler velocimeter (Dantec Dynamics, 55X) with seeding of oil particles of $1 \mu\text{m}$ in diameter. The traverse of LDV is controlled by a 3-axis traverse mechanism with a resolution of $0.5 \mu\text{m}$ in the streamwise (x) and wall-normal (y) directions, and $30 \mu\text{m}$ in the spanwise (z) direction.

The turbulence control experiment is carried out under the bulk mean velocity of $U_m = 3.04$ and 6.78 m/s . The friction velocity, u_τ , is calculated from Dean's empirical equation;

$$u_\tau = \left\{ 0.0365 \left(\frac{2U_m \delta}{\nu} \right)^{-\frac{1}{4}} U_m^2 \right\}^{\frac{1}{2}}. \quad (1)$$

Presently, u_τ is 0.184 and 0.371 m/s at $\text{Re}_\tau = 297$ and 602 , respectively.

2.2 Evaluation of drag reduction

In this experiment, the plasma actuators are installed flush on the bottom of the wind tunnel. Since it is very difficult to measure the wall shear stress at the same time, we use a theoretical identity (FIK identity) delivered by Fukagata et al. (2002), which represents the relationship between the Reynolds stress and the skin friction coefficient, C_f . Based on this, we can evaluate the drag reduction rate by measuring the Reynolds stress under the condition of zero wall-normal velocity, $V = 0$. FIK identity is written as:

$$C_f = \frac{12}{\text{Re}_m} + 12 \int_0^\delta \frac{2}{\delta} \left(1 - \frac{y}{\delta} \right) \left(-\frac{\overline{u'v'}}{4U_m^2} \right) dy, \quad (2)$$

where U_m , δ and ν are the bulk velocity, the half channel-height and the kinematic viscosity, respectively.

2.3 Control system

2.3.1 Control input

We aimed to reproduce experimentally a steady, but spatially periodic control for skin friction reduction as shown in Fig. 2 as proposed by Viptti et al. (2009) and Yakeno et al. (2009). The control input is defined as the following tangential wall velocity:

$$w_{\text{wall}} = w_0 \sin\left(\frac{2\pi}{L} x\right) \quad (3)$$

where w_{wall} is the wall velocity component in the

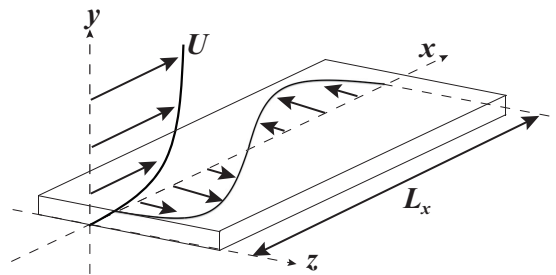


Figure 2: Schematic figure of spanwise-periodic wall transpiration

z -direction on the wall. The parameters to be optimized in Eq. (3) are the amplitude w_0 and the streamwise wavelength L . This control scheme has several advantages such as steady control input, weak parameter dependence of friction drag reduction rate, and relatively large energy saving rate. Yakeno et al. (2009) succeeded in achieving drag reduction up to 45 % when $w_0^+ = 8$ and $w^+ = 1178$ at $\text{Re}_\tau = 150$ in their direct numerical simulation.

2.3.2 Actuator layout

Plasma actuators are fabricated through a MEMS process. It starts with a $525 \mu\text{m}$ -thick Pyrex glass wafer. Upper and lower 300 nm -thick Cr/Au/Cr electrodes are vapour-deposited with a standard lithography process. In order to create periodic control in the near-wall region described by Eq. (3), we use asymmetric surface plasma electrodes as depicted in Fig. 3. The width, a , and length, b , of electrode are 1 mm and 18 mm , respectively. A micro plasma actuator sheet fabricated by this process is shown in Fig. 4.

According to previous work (Forte et al., 2007), it is suggested that, within the plasma region, localized forcing is produced due to the presence of charged particles within a highly non-uniform electrical field. Therefore, it is important to set up densely-arranged plasma actuators in order to mimic uniform disturbance at the wall. However, in order to avoid the parasitic ionization, it is essential to space between sets of upper and lower electrodes. Hence,

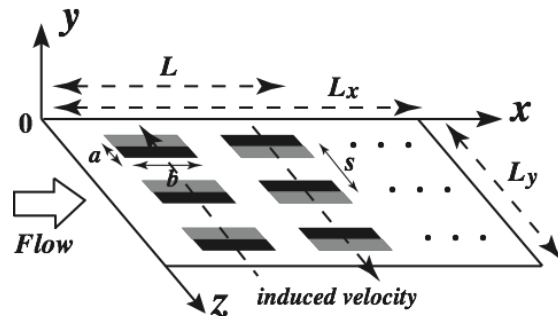


Figure 3: Plasma actuator arrangement to mimic spatially-periodic control

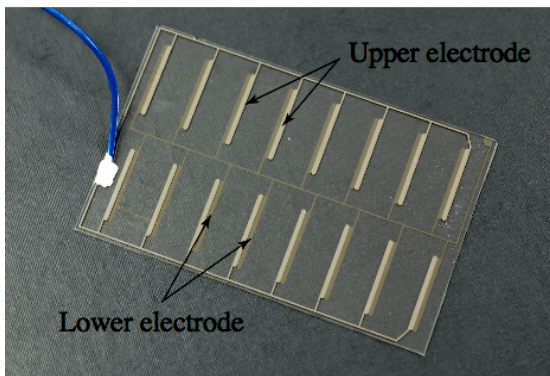


Figure 4: Plasma actuator sheet fabricated by MEMS technique

the interval of each plasma actuator, s , is set to be 10 mm. It is noted that, unlike spatially periodic continuous control input considered in the simulation, the plasma forcing only occurs at discrete locations over the surface and also at a certain height from the solid wall. These actuators are embedded to the bottom wall of the test section of the wind tunnel, where a fully developed turbulent channel flow is established. The gaps between the actuator sheets and the bottom of the wind tunnel are within $\pm 70 \mu\text{m}$.

Hasegawa et al. (2008) demonstrated that over 30 % drag reduction is reached at the time $t^+ > 200$ after the onset of control. This suggests that at least a streamwise length of $L_x^+ \sim 2000$ is necessary to achieve similar control effect considering the typical convection velocity of $U_c^+ \sim 10$ near the wall. In the present experiment, the streamwise and spanwise extents of actuator sheet are 200 and 80 mm, which corresponds to (2400×960) and (4800×1920) in wall units at $Re_\tau = 300$ and 600 , respectively.

In order to achieve dielectric barrier discharge the upper electrode is connected to a high voltage amplifier (HEOPT-5B20-L1) driven by a function generator delivering a sinusoidal waveform. The lower electrode is grounded. A sinusoidal wave voltage V_p with the maximum amplitude up to 5 kV is applied between the electrodes at the frequency f of 5 kHz.

3 Results

3.1 Induced velocity in laminar flow

Previous studies on the use of multiple actuators placed in parallel have shown that one behind the other enhances the induced velocity (Forte et al., 2007). We investigate this phenomenon with the present arrangement of plasma actuators and measure the induced velocity. In order to distribute seeding of small oil particles uniformly in the wind channel and to compensate the wall position, we experimented under the condition of fully developed laminar flow with the center velocity of 0.3 m/s.

Figure 5 shows the measured distribution of induced velocity above the eight actuators (at $y = 0.5$ mm) when discharge is ignited ($V_p = 5$ kV, $f = 5$

kHz). As expected, additional acceleration occurs at each actuator and the spanwise mean velocity, W , progressively increases at $z < 40$ mm, while W changes periodically at $40 < z < 80$ mm. The average of W is about 1.8 m/s, and this amplitude is sufficient large to control wall turbulence since it corresponds to $W^+ \sim 10$ under the condition of $Re_\tau = 300$. As for the wall-normal velocity, V , suction is observed on each actuator, while blowing is observed downstream the actuator. The amplitude of V is about 0.3 m/s, which is much smaller than that in the case of single actuator.

Figure 6 shows the spanwise velocity distribution changing along the streamwise direction. Spatially periodic velocity distribution like a square wave is induced. The boundary layer thickness is $0 < y < 5$ mm, and especially large spanwise velocity is added to the buffer layer as proposed in the numerical simulation (Also see Fig. 7). In this experiment, the spanwise wall disturbance is mimicked by the body fore, which plasma actuators generate. Therefore, W should vanish at the wall, and this is in contrast to the wall velocity assumed in the simulation of Yakeno et al. (2009).

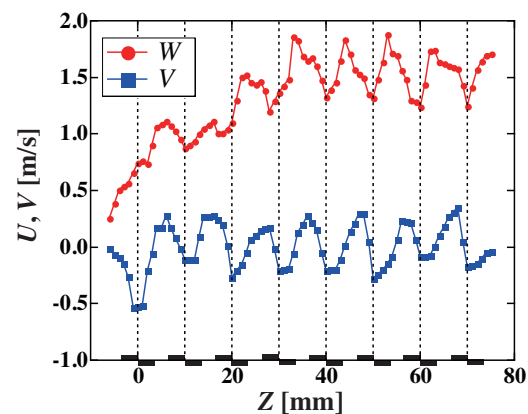


Figure 5: Streamwise and wall-normal velocities above the plasma actuators ($V_p = 5$ kV, $f = 5$ kHz)

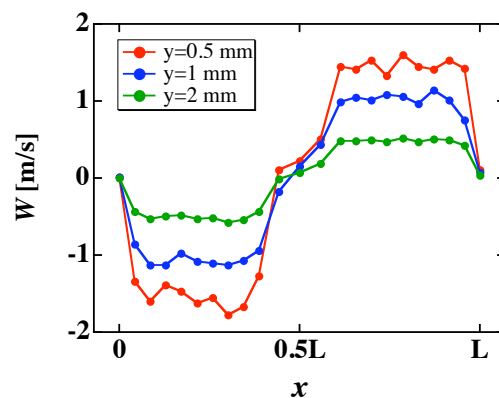


Figure 6: Spatially-periodic disturbance in the streamwise direction ($V_p = 5$ kV, $f = 5$ kHz)

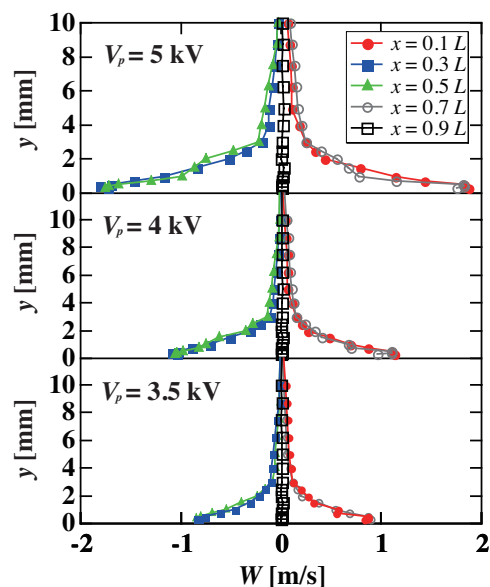


Figure 7: Phase-averaged spanwise velocity with different V_p ($f = 5$ kHz)

3.2 Wall turbulence control at $Re_\tau = 297$

Figure 8 shows the mean streamwise and wall-normal velocities, and the Reynolds stress at different amplitudes of spanwise induced velocity at $z^+ = 480$, which corresponds to the location of one of the plasma actuators arranged. The DNS data (Iwamoto et al., 2002) is also plotted for comparison. In this experiment, W is not measured at the same time, but it is shown in Fig. 7. It is observed that the plasma causes large streamwise velocity acceleration in the buffer region of the boundary layer. The

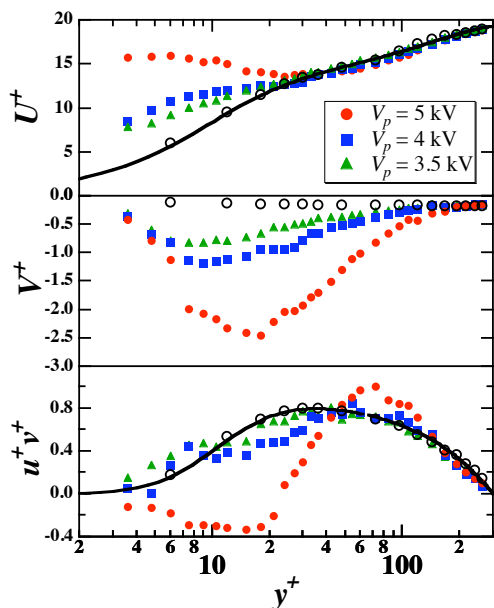


Figure 8: Mean streamwise and wall-normal velocities and Reynolds stress at $z^+ = 480$. (Open circle is no-control experimental data, black line is DNS data)

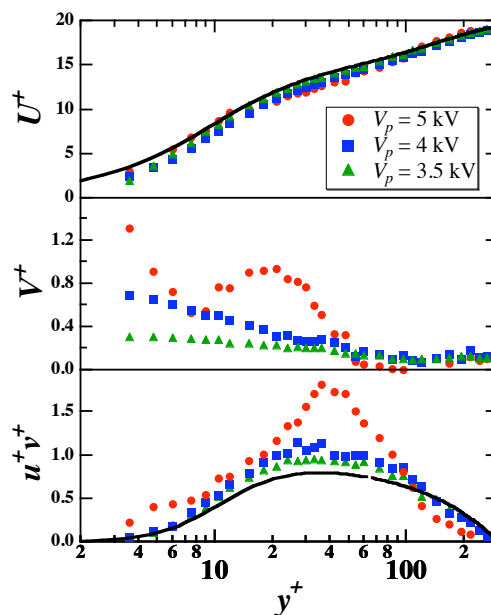


Figure 9: Mean streamwise and wall-normal velocities and Reynolds stress at $z^+ = 540$. (black line is DNS data)

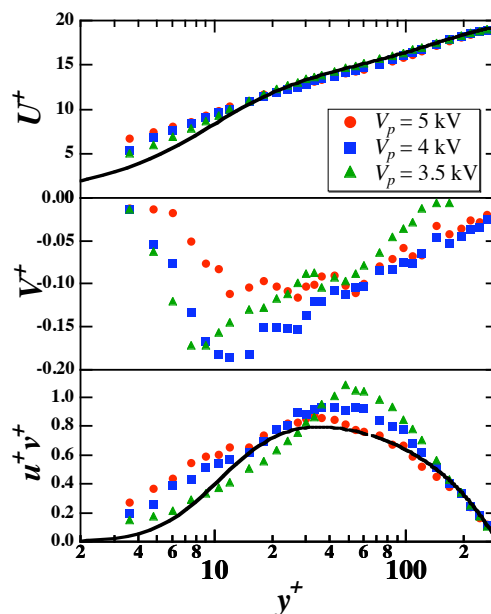


Figure 10: Spatially averaged values of mean streamwise and wall-normal velocities and Reynolds stress (Line is DNS data)

magnitude of the streamwise velocity acceleration becomes larger with increasing the applied voltage. This phenomenon can be explained by the wall-normal velocity. On the plasma actuator, it is well known that strong suction is generated as shown in Fig. 8. As a result, high-speed fluid away from the wall goes down to the near-wall region, and thus the streamwise velocity in the buffer layer is accelerated. Generally, it is known that uniform suction decreases the velocity fluctuations (Park et al., 1999). Therefore, these experimental results show mainly

the influence of local suction.

Figure 9 shows the streamwise and wall-normal velocities at different amplitude of spanwise velocity at $z^+ = 540$, which corresponds to the location in between two neighboring actuators. Unlike the results in Fig. 8, a streamwise deficit is observed in the buffer and logarithmic region. This is because the induced flow is directed away from the wall at this point. Therefore, low-speed fluid is transferred to the center of the channel, resulting in the increase of the turbulence intensities.

Spatial averaged values of experimental data are shown in Fig. 10. The averaged wall-normal velocity, V^+ , is -0.1 , which is very small and nearly identical to the uncontrolled value. Therefore, the friction drag reduction rate can be estimated by using the eq. (3). The estimated drag reduction rate is negative and about -17% , -13% and -2.6% for $V_p = 5, 4$ and 3.5 kV, respectively. The friction drag increases with increasing the applied voltage. Quadrio et al. (2007) examined the effect of a distributed transpiration at the wall with zero-net-mass-flux through DNS, and demonstrated that drag increases except the cases of some selected wavelengths. Therefore, it is expected that the blowing and suction in the spanwise direction result in increase of friction drag.

3.3 Wall turbulence control at $Re_\tau = 602$

A similar experiment is carried out at $Re_\tau = 602$. Figure 11 shows the mean streamwise and wall-normal velocities, and the Reynolds stress at different amplitudes of spanwise induced velocity at $z^+ = 960$, which corresponds to the location of one of the plasma actuators arranged. The same tendency

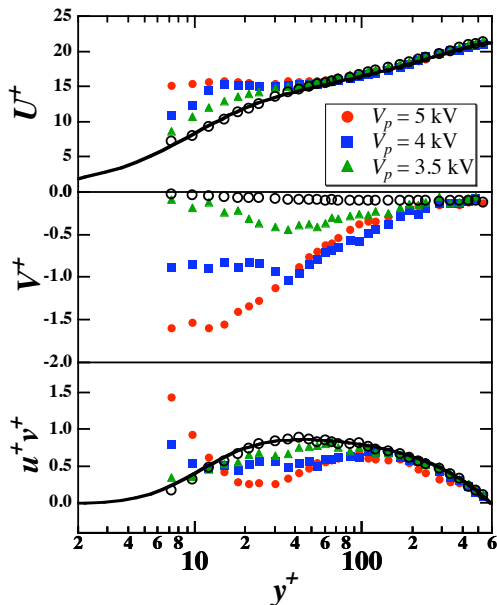


Figure 11: Mean streamwise and wall-normal velocities and Reynolds stress at $z^+ = 960$. (Open circle is no-control experimental data, black line is DNS data)

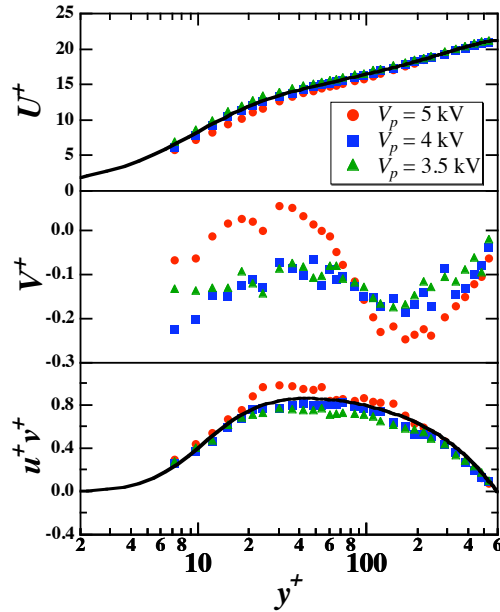


Figure 12: Mean streamwise and wall-normal velocities and Reynolds stress at $z^+ = 1080$. (black line is DNS data)

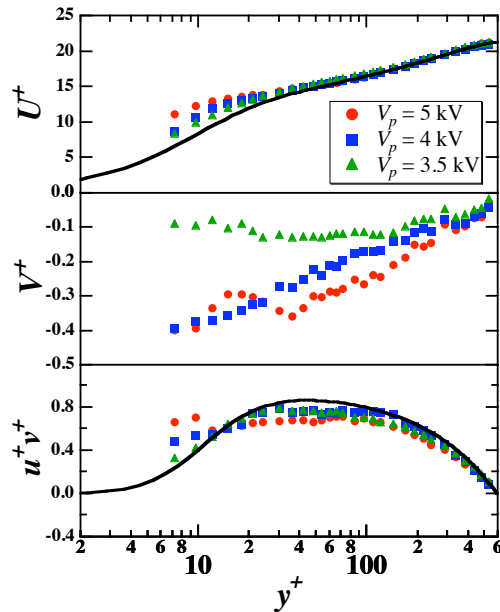


Figure 13: Spatially averaged values of streamwise, wall-normal velocity and Reynolds stress (Line is DNS data)

as that observed at $Re_\tau = 297$ is confirmed. However, in the case of $z^+ = 1080$ as shown in Fig. 12, which corresponds to the location in between two neighboring actuators, the observed amplitude of blowing is weak, so that it is estimated that flow statistics are not remarkably changed in contrast to the case of $Re_\tau = 297$.

Spatially averaged statistics are shown in Fig. 13. On average, suction is induced on the plasma actuator sheet, and an increase of the flow rate is confirmed. Therefore, in the case of $Re_\tau = 602$, it is

not appropriate to evaluate the drag reduction rate by using Eq. (3). The following facts are considered as major reasons for the overall suction. First, the body force induced by the multiple plasma actuators is discrete. Second, the measurement points are limited. Finally, the control is added to the limited area only on the bottom of the wind tunnel. However, these experimental data show that it is possible to cause the remarkable change of flow statistics in turbulent channel flow at low to moderate Reynolds numbers.

4 Conclusions

In the present work, we fabricated the arrayed micro plasma actuators and tried to mimic spatially periodic control input assumed in the previous simulation. We applied the actuators to the turbulent channel flow and assessed their control effect. The major findings are summarized as follows:

1. From the LDV measurement of the flow field, it is found to be possible to induce spatially periodic wall velocity distribution like a square wave by arraying multiple plasma actuators although local body force is induced discretely by each of the plasma actuators.
2. The amplitude of the Stokes layer oscillation induced by the arrayed plasma actuators is sufficient large, so that the periodic spanwise velocity component penetrates even to the buffer layer of turbulent channel flow. According to the previous numerical simulation, these results suggest a possibility of achieving substantial control of wall turbulence with arrayed plasma actuators.
3. Considerable blowing and suction flows exist near the plasma actuator electrodes, so that it is not possible to confirm net drag reduction presently. However, it is found that the plasma actuator array tested offers manipulation of turbulence strong enough to change the turbulence statistics at $Re_\tau = 297$ and 602 .

Acknowledgements

The present work was supported through Grant-in-Aid for Scientific Research (A) (No. 20246036) by MEXT, Japan.

References

Du, Y. and Karniadakis, G. E., (2000), "Suppressing wall-turbulence via a transverse traveling wave," *Science*, Vol. 288, pp. 1230-1234.

Forte, M., Jolibois, J., Pons, L., Moreau, E., Touchard, G. and Cazalens, M., (2007) "Optimization of a dielectric barrier discharge actuator by stationary and non-stationary measurements of the induced flow velocity: application to airflow control," *Exp. Fluids*, Vol. 43, pp. 917-928.

Fukagata, K., Iwamoto, K. and Kasagi, N., (2002), "Contribution of Reynolds stress distribution to the skin friction in wall-bounded flows," *Phys. of Fluids*, Vol. 14, L73-L76.

Hasegawa, Y., and Kasagi, N., (2008), "Effects of Interfacial Wave on Turbulent Mass Transfer in Open Channel Flow," XXII Int. Cong. Theor. Appl. Mech., Adelaide, Australia, August 24-29, 2pp.

Jung, W. J., Mangiavacchi, N. and Akhavan, R., (1992), "Suppression of turbulence in wall-bounded flows by high frequency spanwise oscillations," *Phys. Fluids A*, Vol. 6, pp. 335-359.

Min, T., Kang, S. M., Speyer, J., and Kim, J., (2006), "Sustained sub-laminar drag in a fully developed channel flow", *J.Fluid Mech.*, Vol. 558, pp. 309-318.

Okochi, S., Kasagi, N., Suzuki, Y., and Ito, S., (2009) "Development of Micro Plasma Actuator for Active Flow Control," 7th World Conf. Exp. Heat Transfer, Fluid Mech. and Thermodyn., Krakow, Poland, June 28-July 03, pp. 1741-1748.

Park, J. and Choi, H., (1999), "Effects of uniform blowing and suction from a spanwise slot on a turbulent boundary layer" *Phys. of Fluids*, Vol. 11, p3095-3104.

Quadrio, M., Floryan, J. M. and Luchini, P., (2007), "Effect of streamwise-periodic wall transpiration on turbulent friction drag", *J. Fluid Mech.*, Vol 576, pp. 425-444.

Roth, J. R., Sherman, D. M. and Wilkinson S. P., (1998), "Boundary layer flow control with a one atmosphere uniform glow discharge surface plasma", 36th AIAA Aerospace Sciences Meeting and Exhibit, Reno, NV, 0328.

Viptti, C., Quadrio, M. and Luchini, P., (2009), "Streamwise oscillation of spanwise velocity at the wall of a channel for turbulent drag reduction", *Phys. of Fluids*, Vol 11.

Yakeno, A. Hasegawa, Y. and Kasagi, N., (2009) "Spatio-temporally periodic control for friction drag reduction," *Proc. 6th Int. Symp. on Turbulence and Shear Flow Phenomena*, Seoul, June. 22-24, pp. 598-603.